JOURNAL OF AIRCRAFT
Vol. 38, No. 3, May–June 2001

Dynamic Stall Control by Periodic Excitation, Part 2: Mechanisms

D. Greenblatt,* B. Nishri,† A. Darabi,‡ and I. Wygnanski§
Tel Aviv University, 69978 Ramat Aviv, Israel

Dynamic flow separation and its control over a stationary deflected surface are used to demonstrate the time-scale disparity between the process of dynamic stall, which is dominated by the dynamic stall vortex (DSV), and the excitation-induced large coherent structures that effect its control. Appreciation of this disparity provided a framework for analyzing dynamic stall control on a NACA 0015 airfoil, where leading-edge excitation had effectively eliminated the DSV and significantly attenuated trailing-edge separation. Within this framework, a comparison of static and airfoil phase-locked dynamic pressure data acquired in the vicinity of maximum incidence ($\alpha \approx 25$ deg) revealed that chordwise pressure distributions were independent of the airfoil pitching frequency and that the generation and advection of LCSs were not significantly affected by the dynamic airfoil pitching motion. Furthermore, disparities between static and dynamic data diminished as the excitation frequency increased relative to the airfoil pitching frequency. Oscillations of the aerodynamic coefficients induced by the excitations were negligibly small but served to regulate airfoil cycle-to-cycle disparities typical of the baseline poststall regime.

Nomenclature

C_D	=	drag coefficient, D/cq
C_{Dp}	=	form-drag coefficient, Dp/cq
C_L	=	lift coefficient, L/cq
$C_{L,\max}$	=	maximum lift coefficient
C_M	=	pitching moment coefficient, M/c^2q
C_P	=	pressure coefficient, $(p - p_\infty)/q$
C_μ	=	steady momentum coefficient, J/cq; rms momentum coefficient, $\langle J\rangle/cq$
c	=	airfoil chord
E	=	moment excursion, $C_{M,\max} - C_{M,\min}$
F^+	=	reduced forcing frequency, $f_e X_{\text{te}}/U_\infty$
f_a	=	airfoil oscillation frequency
f_e	=	excitation frequency
g	=	flap gap height
h	=	slot width
J	=	steady jet momentum, $\rho U_J^2 h$
$\langle J\rangle$	=	rms jet momentum, $\rho\langle u_J\rangle^2 h$
k	=	reduced airfoil pitching frequency, $\pi f_a c/U_\infty$
L_f	=	flap length
M	=	Mach number
p	=	local pressure
q	=	freestream dynamic pressure, $\rho U_\infty^2/2$
Re	=	chord Reynolds number, $\rho U_\infty c/\mu$
Re_f	=	flap Reynolds number, $\rho U_\infty L_f/\mu$
t	=	time
U_ϕ	=	large coherent structure phase velocity
u, U	=	oscillatory, mean velocity
X_{te}	=	distance from slot location to trailing edge
x/c	=	normalized chordwise distance
x_B	=	recirculation bubble length
α	=	instantaneous incidence angle
$\bar{\alpha}$	=	mean incidence angle
δ	=	flap deflection angle
μ	=	air dynamic viscosity
ρ	=	air density
τ	=	dimensionless time, tU_∞/L_f or tU_∞/c
ϕ	=	phase angle
$\langle\,\rangle$	=	rms quantity

Subscripts

A	=	allowable excursions
r	=	conditions at reattachment with excitation
$r0$	=	conditions at natural reattachment
s	=	conditions at separation with excitation
st	=	static stall
$s0$	=	conditions at natural separation
∞	=	freestream conditions

Superscript

a'	=	oscillatory component of a

I. Introduction

FLOW separation can be delayed and reattachment effected, by periodic addition of momentum with or without the concomitant superposition of mass flux.[1–3] This method is much more effective than traditional steady blowing and at times represents a saving of two orders of magnitude in the momentum coefficient required to achieve a prescribed improvement in performance.[2,3] The actuators required may, thus, be autonomous and decoupled from the main propulsive systems. The basis for this method of flow control was discovered by Schubauer and Skramstad,[4] who introduced periodic perturbations in a laminar boundary layer to trigger a known instability, that is, to initiate Tollmien–Schlichting waves. Their technique[4] not only became a major diagnostic tool in transition research, but also led the way to the control of separation by periodic excitation. Although laminar–turbulent transition could be effected at low Reynolds numbers by introducing periodic perturbations,[5] the manipulation of turbulent shear flows was traditionally considered unattainable because of the belief that turbulence is a random process. However, observations such as those of Brown and Roshko[6] in the mixing layer demonstrated that large coherent structures (LCSs) are responsible for the transport of momentum across the flow domain. Moreover, the introduction of periodic excitation at the flow origin (e.g. splitter plate trailing edge) is an efficient and convenient

Received 11 December 1998; revision received 6 September 1999; accepted for publication 8 September 2000.

*Postdoctoral Fellow, Department of Fluid Mechanics and Heat Transfer, Faculty of Engineering. Member AIAA.

†Research Associate, Department of Fluid Mechanics and Heat Transfer, Faculty of Engineering.

‡Graduate Student, Department of Fluid Mechanics and Heat Transfer, Faculty of Engineering.

§Lazarus Professor of Aerodynamics, Department of Fluid Mechanics and Heat Transfer, Faculty of Engineering; currently Professor of Aerospace Engineering, Department of Aerospace and Mechanical Engineering, University of Arizona, Tucson, Arizona 85721-00119. Fellow AIAA.

method for the control of mixing.[7] Excitation accelerates and regulates the generation of LCSs, particularly when the mean flow is unstable, thereby transferring high-momentum fluid toward the surface. This process forms the basis of separation control by periodic excitation.[1,2]

A detailed parametric study of forced separation control was carried out[2] and was followed by extensive experiments on a wide range of airfoils including flap deflections[3,8] and sweep[9] at various Reynolds numbers ($10^5 \leq Re \leq 5 \times 10^7$) (Ref. 10) and Mach numbers ($M \leq 0.4$) (Ref. 11) and was tested on a small uncrewed air vehicle.[12] These observations confirmed the universality of excitation on stationary wings in steady flow and paved the way for possible control of dynamic stall. The dominant feature of dynamic stall on a thin airfoil is a strong vortical flow, which begins near the leading-edge, grows, and forms a vortex that is then swept downstream. This dynamic stall vortex (DSV) brings about losses in lift, sharp increases in drag, and destructive pitching moments.[13] Consequently, all research into dynamic stall suppression focuses on controlling or eliminating the DSV. Typically, some form of airfoil geometry modification is made, for example, leading-edge slat,[14,15] or boundary-layer control is employed, for example, blowing[16] or suction,[17] where these changes are geared specifically to the leading-edge region where the vortex originates. Presently, attempts to contain the DSV are still confined to the laboratory and have not, as yet, been applied in practice.

The need to understand and predict dynamic stall, and the DSV in particular, has long been considered a prerequisite to effective control. This viewpoint has motivated numerous experimental and numerical investigations during the last two decades. With advances in experimental techniques, for example, particle image velocimetry (PIV),[18] this decade has witnessed a deeper understanding of the initiation and development of dynamic stall, as well as the effect of compressibility, for example, point diffraction interferometry.[19,20] Advances in computer power, algorithms, and modeling have fueled computational progress to the point where quantitative predictions of time-dependent aerodynamic loads are becoming a reality.[21,22] Notwithstanding these advances, our inability to effect control has remained a major stumbling block in the way of advanced rotor development.[23,24] Recently, however, the method of oscillatory excitation[25–27] was demonstrated as a technology capable of controlling compressible dynamic stall and significantly improving dynamic airfoil performance. This led to a detailed parametric study, the subject matter of the companion paper,[28] which focuses on mapping the effect of a wide variety of parameters on dynamic stall control, and provided the motivation for the analysis presented here.

The principal objective of this paper is to study the mechanisms that effect dynamic stall and its control. The parameters governing steady separation control are initially discussed and the time-resolved mechanisms that effect that control are presented in Sec. II. This is followed by a description of classical DSV development and the analogy between dynamic stall simulation (and its control) on a stationary deflected flap with classical airfoil dynamic stall (Sec. III). This characterization illustrates the pivotal importance of the different timescales associated with dynamic stall vs those of the controlling LCSs. Finally, this characterization provides a framework for analyzing dynamic stall control on an airfoil and illustrates the manifestation of timescale delineation on the mechanisms governing dynamic stall control (Sec. IV).

II. Separation Control by Excitation

A. Governing Parameters

Consider a generic-flap configuration (Fig. 1), where the upstream boundary layer is turbulent and disturbances are introduced by zero net mass-flux two-dimensional jet excitation flow. Dependent variables, such as bubble-length x_B or C_P describing the state of the over the flap are primarily functions of the variables $\Delta\delta$, x/L_f, F^+, and C_μ. Full details of the experiment and detailed parametric study may be found in Ref. 2. The parameter $\Delta\delta$ describes a deflection that exceeds the angles at which separation or reattachment occur naturally, that is, $\Delta\delta_s = (\delta - \delta_{s0})$, $\Delta\delta_r = (\delta - \delta_{r0})$. In this way

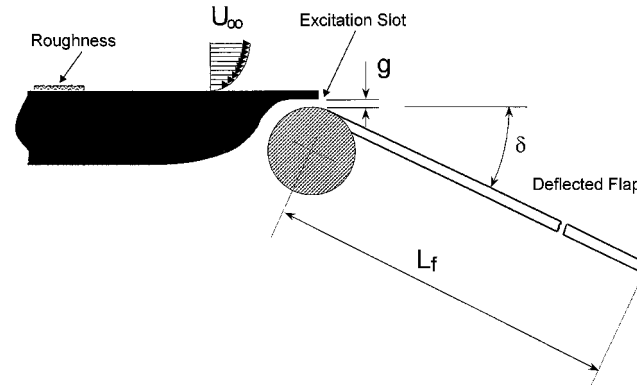

Fig. 1 Schematic of the generic-flap and shoulder region.

the initial condition of the flow is accounted for because δ is either referred to as δ_{s0} (the angle at which separation occurs in the absence of periodic excitation) or to δ_{r0} (the angle at which reattachment occurs). Furthermore, the total momentum coefficient is designated $C_\mu = (c_\mu, \langle c_\mu \rangle)$ and is used throughout to denote either steady momentum c_μ or periodic excitation $\langle c_\mu \rangle$.

The introduction of two-dimensional, periodic oscillations into a turbulent boundary layer enables it to resist larger adverse pressure gradients without separating. The optimum reduced frequency for attaching the flow to a straight surface is $F^+ \approx 1$ and is linked to neutral stability of the separated mixing layer.[2] After reattaching, the flow encloses a large bubble, whose size may be reduced by increasing F^+ or C_μ. The most effective frequencies for separation prevention are $2 \lesssim F^+ \lesssim 4$ (approximately less than or equal to). At high excitation frequencies, the flow separates from the trailing edge because the LCSs dissipate before reaching the end of the flap. Hysteresis between attached and separated conditions is typical to this bistable flow, and it may be induced not only by changing δ, but also by changing F^+ and C_μ. In general, the ratio between the $\langle C_\mu \rangle_r$ required for reattachment and the $\langle C_\mu \rangle_s$ needed to prevent separation may be larger than an order of magnitude.

B. Basic Mechanisms

On reattachment, due to periodic excitation at $F^+ \sim \mathcal{O}(1)$, the mean bubble dimension is commensurate with the length of the flap, and a similar bubble may exist just before complete separation. The time-average pressure distribution shown in Fig. 2a for $C_\mu = 0.01\%$ is indicative of this situation, where there is an almost constant pressure region extending up to 30% of the flap length, followed by an increase in pressure up to the trailing edge. Flowfield measurements with PIV show time-mean vorticity contours (Fig. 2b), and the mean streamline $\bar{\psi} = 0$ indicated that the bubble dimensions vary between 40 and 55% of L_f depending on the value of C_μ used for the prescribed $(\delta - \delta_{s0})$. The flow can be maintained in this state as long as the C_μ supplied provides a sufficient margin of safety to prevent separation by a bubble-bursting mechanism. Because the flow bounding the bubble is no different from the familiar mixing layer (at least over the initial, constant pressure length),[7] an increase in the excitation frequency shortens x_B for two reasons. First, the streamwise distance between successive rolled-up vortices decreases, and second, these structures dissipate closer upstream than those generated at lower frequencies. As a consequence, there is a limit to separation control by further increasing the excitation frequency because the effectiveness of the momentum transfer mechanism diminishes over the increasing distance between the reattachment location and the trailing edge of the flap. Thus, separation reoccurs when the local disturbance amplitude falls below the threshold level required for that deflection angle (provided $\delta > \delta_{s0}$). Under these circumstances, separation commences near the trailing edge, where the amplitudes of the imposed perturbations have dissipated.

The pressure distribution over the flap, when the amplitude of the imposed perturbations was decreased to the minimum level necessary to keep the flow attached, that is, to $C_\mu \approx 10^{-3}\%$, is very

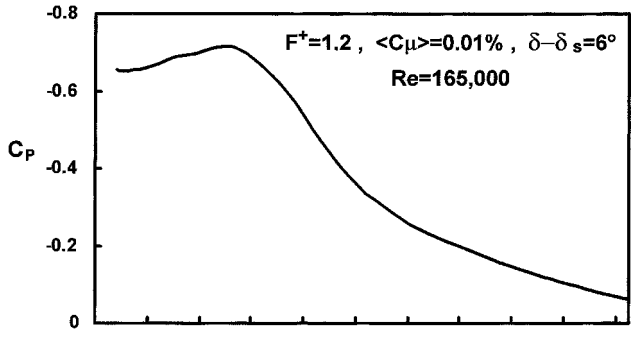

a) Time-mean pressure distribution

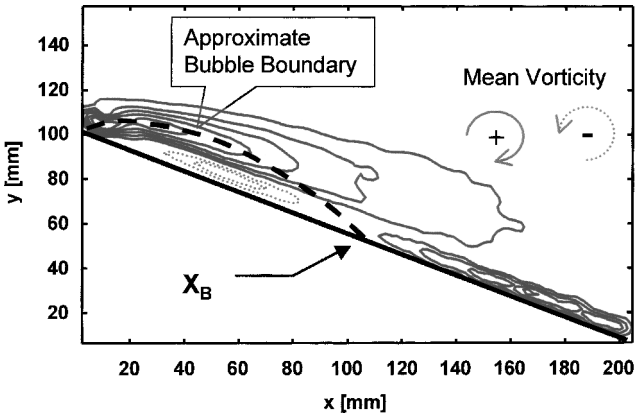

b) Vorticity contours

Fig. 2 Approximate bubble size $\bar{\psi} = 0$.

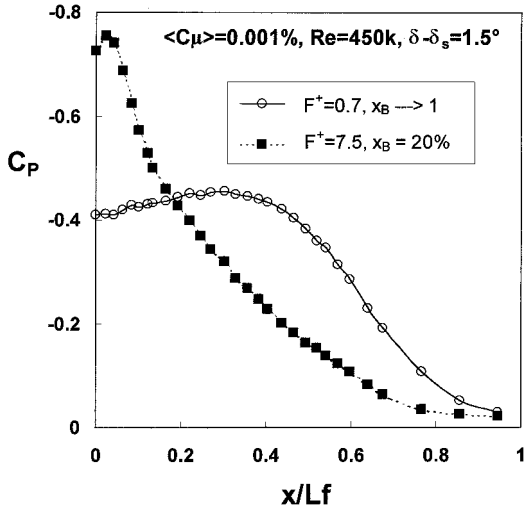

Fig. 3 Time-mean pressure distribution on the flap at two reduced excitation frequencies.

sensitive to F^+. Two limiting cases are shown in Fig. 3. At $F^+ = 0.7$, the reduction in amplitude generated a mean bubble, whose dimensions were commensurate with the length of the flap. Thus, a small additional increase in the bubble length caused it to burst. In this case the flow is already separated over most of the flap in spite of the large normal force it generated. At $F^+ = 7.5$ the size of the bubble was insignificant, but the boundary layer at the trailing edge was thick and depleted of momentum. Thus, a small reduction in C_μ caused separation, which propagated upstream from the trailing edge.

Although the resulting time-mean flowfield is of primary practical importance, it belies the generation and evolution of the LCSs, which are its very basis for existence. Insight into this process, which is independent of Reynolds number, is provided by phase-locked PIV

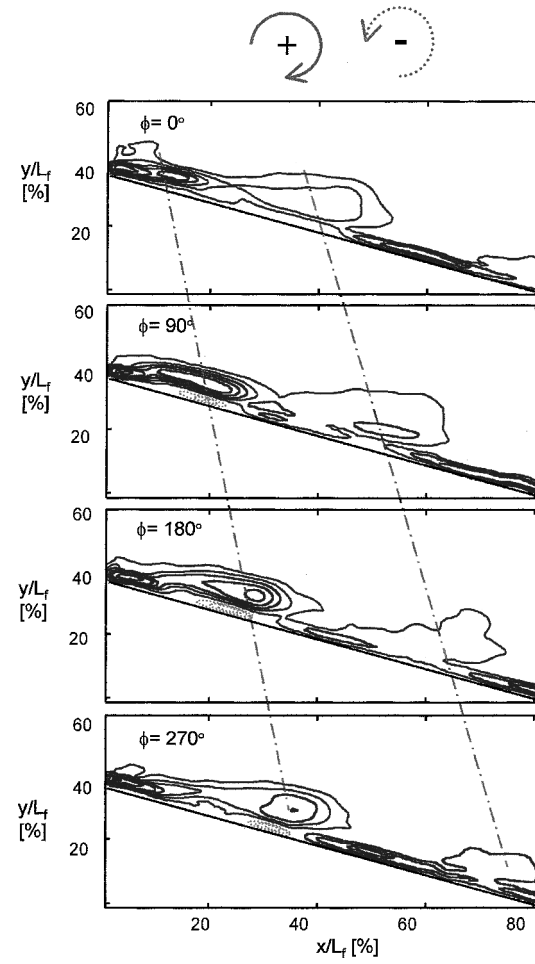

Fig. 4 Phase-locked vorticity contours on the flap within the excitation cycle; same conditions as Fig. 2.

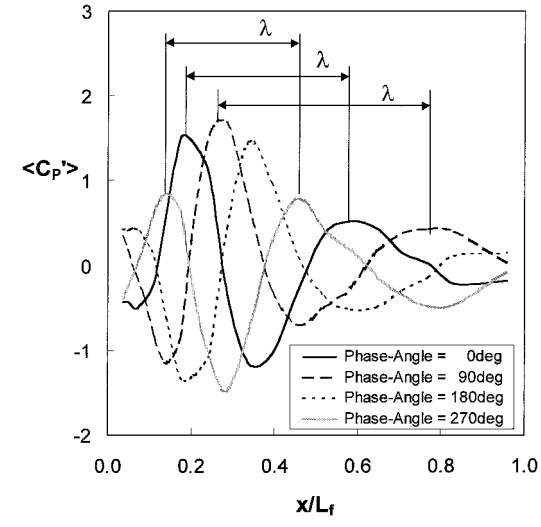

Fig. 5 Phase-locked oscillatory pressure distributions on the flap within the excitation cycle, indicating the increasing wavelength λ; same conditions as Fig. 2.

vorticity measurements (Fig. 4) and phase-locked surface pressures (Fig. 5). Figure 4 shows the high degree of structural coherence near the origin of excitation, as well as the relatively slow moving structures in this region. Farther downstream, the structures dissipate due to turbulent diffusion with a concomitant increase in their phase velocities. Thus, the apparent time-mean recirculation bubble is, for the most part, a manifestation of these traveling structures. These observations are reflected by phase-locked pressure data, which indicate

the progressively increasing wavelength with distance along the flap (Fig. 5). The high degree of vorticity coherence is associated with relatively large surface pressure excursions and the increasing phase velocity $\lambda \cdot f_e$.

III. Basis of Dynamic Stall and Its Control

A. Formation of the DSV

Computer simulations,[29,30] together with experimentation,[31] reveal broad consensus regarding the dominant flow states (approximately four)[32] in the DSV development. Stage I entails a (thin) layer of reversed flow in the leading-edge region in which fluid particles are driven in the reverse direction as a direct result of the strong adverse pressure gradient. This is followed by the so-called primary recirculation region (Van Dommelen–Shen interaction),[29] where faster moving (reversing) particles collide with slower moving particles ahead of them, resulting in the movement of the fluid particles away from the wall. This gives rise to counterclockwise secondary recirculation region (stage III)[30] associated with strong viscous/inviscid interaction[31] and focusing or concentration of surface layer vorticity.[32] Primary and secondary recirculating regions interact (stage IV), ejecting fluid in an eruptive plume[32] from the wall, thereby initiating the breakaway[29] and ultimate formation[30] or rollup[32] of the dynamic stall vortex.

The timescale associated with the four-stage process is governed by the airfoil oscillation rate. For rotorcraft, the process typically takes place over the dimensionless time interval $\tau \equiv tU_\infty/c = \mathcal{O}(10)$.

B. Simulation of Dynamic Stall and Its Control

DSV formation and the process of dynamic stall, described in the preceding section, can be simulated on a stationary generic flap (see Sec. II), in the following manner. Consider the forced reattachment of a boundary layer to a flap under the conditions $F^+ = 3$, $(\delta - \delta_{s0}) = 5$ deg, and $C_\mu = 0.04\%$. At time $t = 0$, C_μ is reduced abruptly from 0.04% to 0. Instantaneous pressure data are then sampled and phase averaged to determine the dynamic changes that occur during the transient event. It is expedient to define the dimensionless time $\tau = tU_\infty/L_f$ and to note that because the LCSs propagate over the flap during the time interval $L_f/U_\phi \approx 2L_f/U_\infty$ then $\tau \approx 2$ characterizes the time of flight over the flap. At the instant $\tau = 2$, after the cessation of excitation, the flap boundary layer remains attached.

An analogous scenario is that of a thin airfoil pitching past the static stall angle[33]; thus, in both cases, at an instant marked by $\tau = 0$, we have attached flow in a natural (unforced) poststall regime. Figures 6a and 6b compare the static flap with airfoil dynamic stall for C_L and C_M, on the basis of τ, where $\tau = tU_\infty/c$ for a NACA 0012 airfoil with $\alpha = 9 + 5\sin(\omega t - 90)$ deg, $k = 0.05$, and $Re = 0.24 \times 10^6$. Note that the flap data are plotted from cessation of forcing whereas the airfoil data are plotted from $\alpha \geq \alpha_s$ during one-half of the pitch cycle. Notwithstanding the quantitative C_L and C_M differences between the flap and airfoil, the overall trends are markedly similar. The vortex formation on the pitching airfoil is apparent from the increase in lift with simultaneous drop in the one-quarter chord pitching moment. The same phenomenon is apparent on the stationary flap. Following lift stall, the moment for both airfoil and flap increase, because the flow tends toward reattachment in the former case, whereas total separation prevails in the latter. The pressure distributions over the airfoil and flap illustrate the same basic trend namely, a sharp drop in C_P near the leading edges, accompanied by a more moderate increase in C_P over the large remainder of the chord (not shown).[33]

Figure 6 also indicates the extent of one-half of the LCS dimensionless time $\tau = 1$ and contrasts this with the airfoil half-cycle time $\tau = 32$. Of crucial importance here is that the DSV and LCS timescales (or frequencies) differ by a factor of about 30, whereas the detailed comparison is of secondary importance. This result forms the basis of the stark contrast between the destructive nature of the DSV and separation-suppression attribute of excitation. The experiment was repeated at different freestream velocities and flap

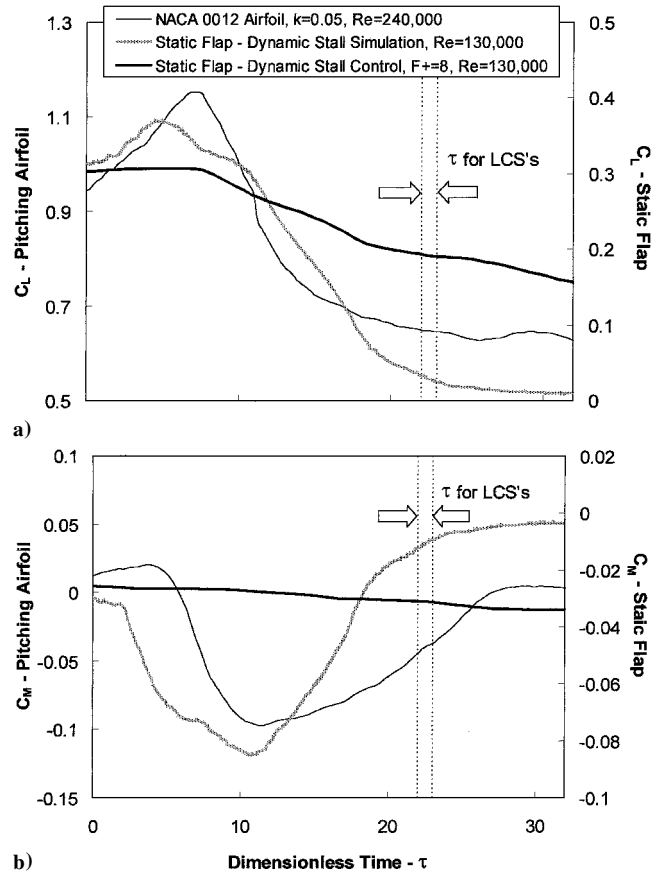

Fig. 6 Dynamic stall, and its control, on a stationary flap.

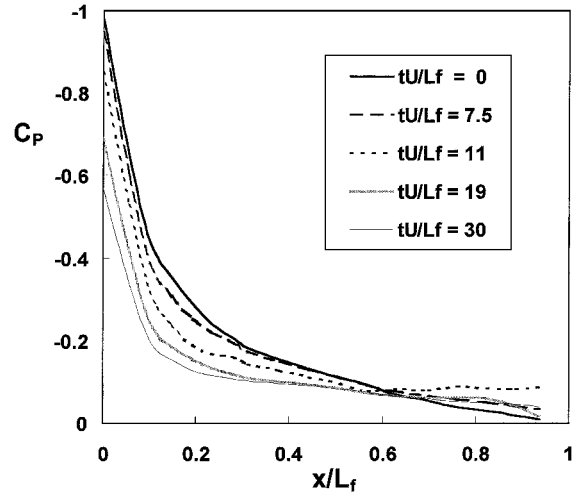

Fig. 7 Stationary flap pressure distributions during dynamic stall control.

lengths with the data scaling at the appropriate ratios confirming its repeatability.

To illustrate simulated dynamic stall control, consider the aforementioned scenario where the frequency is abruptly changed from $F^+ = 3$ to 8 while maintaining $C_\mu = 0.04\%$ and considering the data on the same basis as before (Figs. 6 and 7). The separation due to the high-frequency excitation was completely different, with effective elimination of the DSV and its associated increase in $|C_P|$ before complete separation. For this case, separation commenced from the trailing edge (see Sec. II) because the amplitude associated with the structures at high F^+ did not suffice to maintain attached flow and proceeded upstream with increasing time (Fig. 7). Here, the minimum C_P at the leading edge was not affected during the initial stages

of the process, $\tau \leq 5$, and as the separated region propagated toward the leading edge, it diminished somewhat but was still significant at $\tau > 20$. In fact the flow over the leading 10% of the flap remained attached at all times. More important, the integrated lift force and moment (Fig. 6) gradually changed to the values appropriate to the new imposed excitation conditions, without the dramatic lift increase and moment excursion, thereby confirming the effective control of the DSV. The difference in the end state between separation at $C_\mu = 0$ and 0.04% at $F^+ = 8$ is due to a small region of attached flow at the leading edge whose dimension depends on the excitation frequency.

IV. Control of Airfoil Dynamic Stall

A. Experimental Setup and Procedure

Experiments were performed on a NACA0015 airfoil (610 span × 365 mm chord) equipped with 36 pressure taps and a 0.25c trailing-edge flap.[28,33] The airfoil contained an interior plenum and a 0.5 mm tangential leading-edge slot to effect flow excitation, and the flap was not deflected ($\delta = 0$ deg) for all data presented in this paper. The airfoil was pitched about the one-quarter chord position, with ±5 deg excursions in incidence angle, and dynamic pressure measurements were made with a multichannel array of pressure transducers. Flow excitation was achieved by means of a rotating valve and a small centrifugal blower connected to the airfoil plenum chamber. The large timescale disparity, discussed earlier, established a framework for analyzing the surface-pressure data, which could be phase locked to both airfoil and excitation frequencies. Note that, because $f_e \gg f_a$, no phase relation was enforced between excitation and pitching oscillations.

B. Discussion of Results

Upper surface airfoil pressures phase averaged with respect to the airfoil oscillation, as a function of normalized distance and time is presented in Figs. 8a–8c, for the baseline configuration, for $F^+ = 1.1$, and for $F^+ = 0.6$ cases, respectively. The corresponding leading- and trailing-edge pressures appear in Fig. 9. These reduced frequencies were selected due to their consistently good performance for a wide range of conditions.[28] The airfoil incidence angle varied as $\alpha = 20 + 5\sin(\omega t - 90)$ deg, entirely in the static poststall regime, with $k = 0.1$ and $Re = 0.3 \times 10^6$. For the baseline case (Fig. 8a), the DSV forms when $\omega t \approx 90$ deg corresponding to $\alpha \approx 20$ deg, while concomitantly the pressure decreases near the trailing edge. At $\omega t > 90$ deg, the leading-edge pressure increases while the trailing-edge pressure continues to decrease, suggesting gross separation in the trailing-edge region. Although the overall effect on lift would be small, the redistribution of pressure results in a nose-down pitching moment for the phase $90 > \omega t > 180$ deg (corresponding to $20 > \alpha > 25$ deg on the upstroke). At $\omega t > 180$ deg, the DSV moves down the airfoil surface resulting in a complete leading-edge stall for $180 > \omega t > 270$ deg (corresponding to $20 > \alpha > 25$ deg on the downstroke), with further concomitant trailing-edge pressure decrease. The leading-edge pressures begin recovering when $\omega t \gtrsim 300$ deg, and the airfoil experiences an increase in lift toward the end of the pitch cycle.

In contrast to the preceding discussion, no significant vortex formation is experienced with excitation at $F^+ = 1.1$ or 0.6 with $C_\mu = 0.1\%$ (Figs. 8b and 8c). This is apparent from the leading-edge pressures that fall only slightly beyond $\omega t > 90$ deg. However, higher leading-edge suction is attained for $F^+ = 1.1$ over virtually the entire cycle. In both cases, trailing-edge separation is significantly attenuated, particularly between $90 > \omega t > 300$ deg. The higher frequency appears to be more effective in this regard for $120 < \omega t < 270$ deg, that is, in the vicinity of maximum α, whereas the opposite is true at lower α. A comparison of the leading- and trailing-edge pressures also indicates that the $F^+ = 1.1$ case has a larger harmonic content than that at $F^+ = 0.6$.

Pressure distributions, phase averaged with the dynamically pitching airfoil ($k = 0.1$), at $\alpha = 25$ deg ($\omega t = 180$ deg) are compared with static data at the same incidence angle for the baseline as well as for the low ($F^+ \lesssim 1$) and high ($F^+ \gtrsim 2$) excitation frequencies (Figs. 10a and 10b, respectively). For the static baseline case, the flow is separated over the entire airfoil with $C_P \approx -1$ throughout whereas the dynamically pitching airfoil has entered into dynamic stall with a DSV being generated at $x/c < 0.05$, near the leading edge (cf. Fig. 8a). Consequently, the lift generated in the dynamic case is higher ($CL = 1.26$ vs 0.82), and the dynamic moment changes rapidly at $\alpha = 25$ deg due to the movement downstream of the DSV. In the forced static case, the flow does not separate near the leading edge, generating locally a $C_P = -5$; rather, it continuously sheds vortices at the frequency of excitation. The addition of pitching motion does not alter this shedding in any material way, even at the low F^+ considered (Fig. 10a). The overall agreement between the static and dynamic data is good with only minor differences near the leading edge (at $0.1 < x/c < 0.3$ for $F^+ = 1.1$ and $x/c < 0.05$ for $F^+ = 0.6$). Although the leading-edge suction peak is larger for $F^+ = 1.1$ (cf. Figs. 8 and 9), $F^+ = 0.6$ generates a larger normal force (and hence larger lift) as a result of the more gradual pressure recovery shown (Fig. 10a). These data are qualitatively consistent with the observations on the flap (see Sec. II), and consequently it is

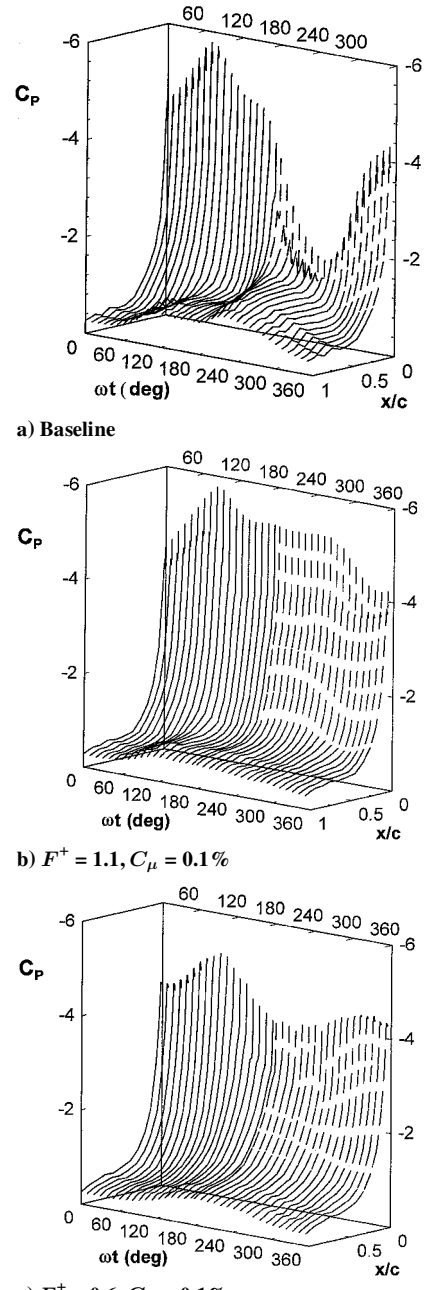

Fig. 8 Upper surface airfoil pressure distributions.

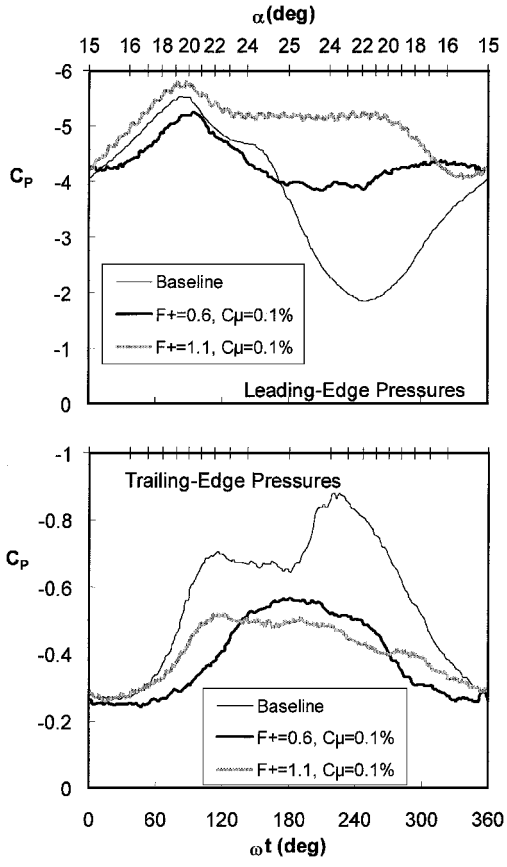

Fig. 9 Leading- and trailing-edge pressures during the airfoil oscillation cycle.

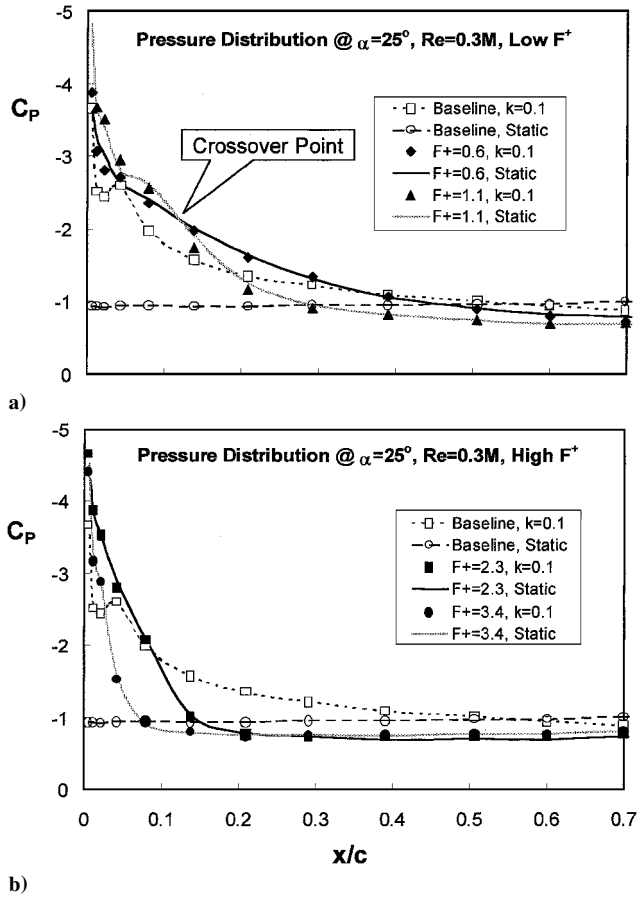

Fig. 10 Comparison of static time-mean and dynamic phase-locked upper-surface pressure distributions at maximum incidence.

assumed that a relatively large, oscillating bubble is enclosed on the airfoil surface at the lower frequency. At high excitation frequencies (Fig. 10b), the pressure recovery length shortens with increasing F^+. The higher reduced frequencies $F^+ = 2.3$ and 3.4 were less effective in increasing lift and containing moment excursions (as shown in Ref. 28) due to their inability to keep the boundary layer attached at this input of C_μ beyond $x/c > 0.2$ and 0.1, respectively. However, at these higher frequencies, the static and dynamic pressure distributions were also indistinguishable. In this case, the flow near the trailing edge was stalled.

Note that separation control on the generic flap (see Sec. II) is idealized, with a turbulent upstream boundary layer, no secondary stream on the lower surface and its associated vortex shedding, no surface curvature, and a well-defined separation location at the flap knee. On the airfoil, the upstream boundary layer is highly accelerated and laminar, there is significant curvature, particularly in the leading-edge region, and the boundary layer is partially separated in the trailing-edge region with opposite vorticity being intermittently shed into the wake. Therefore, there are quantitative differences between the mean flap and airfoil pressures (cf. Figs. 3 and 10a) as well as phase-locked pressures (cf. Figs. 5 and 11a). However, the qualitative similarity as well as the similar F^+ dependence indicate that the mechanisms responsible for separation delay are alike in both cases. Given these similarities, the traditional notion of boundary-layer transition forcing local reattachment is inappropriate when considering separation delay by excitation.

Figures 11a and 11b compare static and dynamic oscillatory pressures C_P' at different phases of excitation on the airfoil surface, indicating the amplitude and phase velocity of the LCSs. The static data (lines) are for $\alpha = 25$ deg, and the dynamic data (symbols) were generated from a time window restricted to $24.5 \leq \alpha \leq 25$ deg, including portions of the upstroke and downstroke pitching motion, from which the ensemble averaged C_P had been removed. From

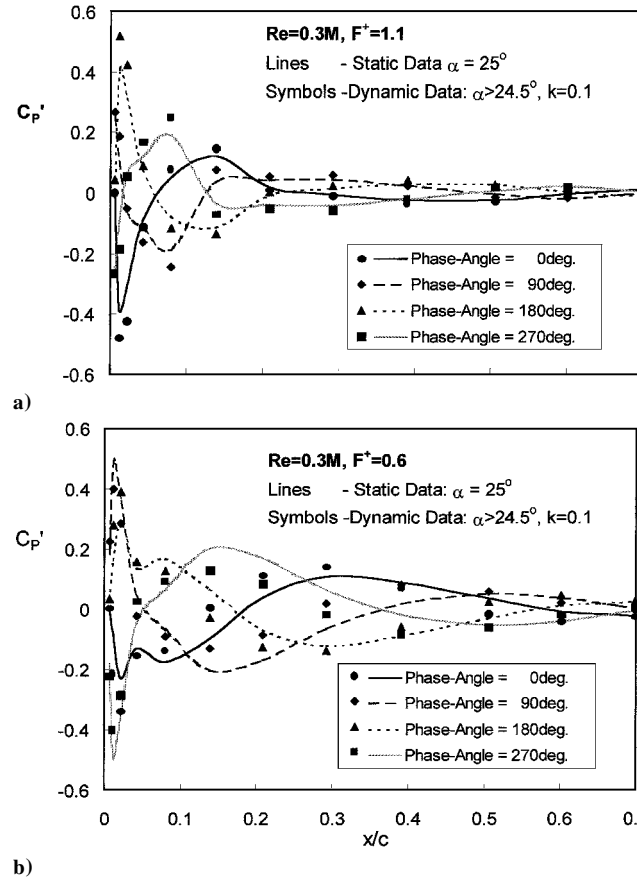

Fig. 11 Comparison of oscillatory pressures at maximum incidence for the static airfoil and in the vicinity of maximum incidence for the dynamically pitching airfoil.

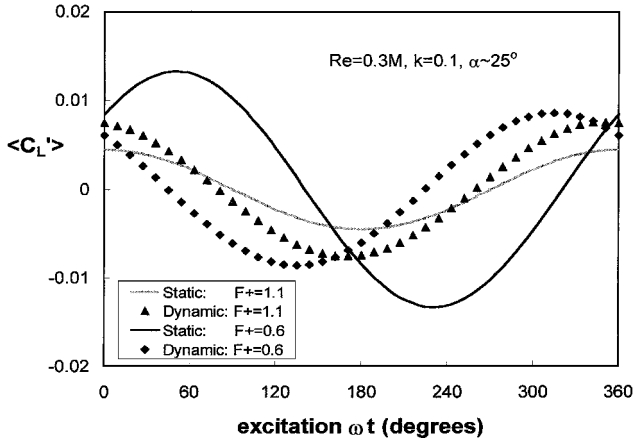

Fig. 12 Oscillatory lift induced by excitation at maximum incidence for the static airfoil and in the vicinity of maximum incidence for the dynamically pitching airfoil.

Fig. 11a, the static and dynamic LCSs have essentially the same phase velocities. However, at $0.01 < x/c < 0.15$, the peaks of the pressure excursions on the dynamically oscillating airfoil are larger than for the static case. This may be due to the varying incidence angle, but could also be caused by changes in the generation of the LCSs between 24.5 and 25 deg due to maximum airfoil acceleration at maximum incidence. The same trend is evident when $F^+ = 0.6$, but only at $x/c < 0.05$ (Fig. 11b). At $0.05 < x/c < 0.4$, however, the reverse trend is observed, that is, the excursions in pressure for the static case overshoot those obtained during airfoil pitching. Both amplitude and phase velocity are affected, most probably because the excitation frequency f_e is only 18 times larger than the airfoil pitch rate f_a. Note also that the amplitude of the oscillatory pressure component is larger for $F^+ = 1.1$ than for $F^+ = 0.6$ at $x/c \gtrsim 0.1$, whereas for $0.1 \lesssim x/c > 0.7$ the opposite is true. This observation ties in directly with the pressure crossover point shown in Fig. 10a, providing a rudimentary explanation for the higher lift force generated at the lower frequency.

Figure 12 shows the fluctuating component of C_L induced by the LCSs over the excitation cycle at two reduced frequencies with static data at $\alpha = 25$ deg and dynamic data restricted to $24.5 \leq \alpha \leq 25$ deg as before, that is, the integrated data from Figs. 11a and 11b. For $F^+ = 1.1$, the dynamic and static data have similar amplitude and phase shifts, with the dynamic data amplitudes somewhat larger than those for the static data. This is due to the larger amplitudes at $0.01 < x/c < 0.15$ in Fig. 11a. For $F^+ = 0.6$, there are significant differences between static and dynamic amplitudes and phase shift that is approximately 100 deg. However, even for the worst-case scenario, excitation produces almost negligibly small oscillatory loads on the airfoil with $\Delta C_L/C_{L,\max} < 1\%$, $\Delta C_M/E_A \approx 4\%$, and $\Delta C_{Dp}/C_{Dp}$ (mean) $\approx 2\%$ (Ref. 33). This confirms the static airfoil data of Seifert et al.[3] and Darabi,[34] who observed that for $F^+ \approx 1$ there are at least two vortices present on the airfoil upper surface at any instant. Moreover, these observations show that, at higher excitation frequencies, a greater number of vorticies are resident on the airfoil, and this serves to reduce oscillatory loads associated with vortex shedding.

The effect of airfoil reduced frequency k on excitation performance is assessed in Figs. 13a–13c for $F^+ = 0.6$. Figures 13a–13c indicate that the baseline data are significantly affected by k, particularly during the downstroke part of the cycle. Excitation, however, significantly reduces the dependence of the aerodynamic coefficients on k, with essentially the same excursions and time history for all coefficients. Similar observations were made with $F^+ = 1.1$ (Ref. 33).

A comparison of phase-averaged aerodynamic quantities to those measured instantaneously is presented in Figs. 14a–14c. During the upstroke, the differences between phase-averaged and instantaneous data are relatively small for both baseline and excited cases. Near maximum incidence and during the downstroke, however, large

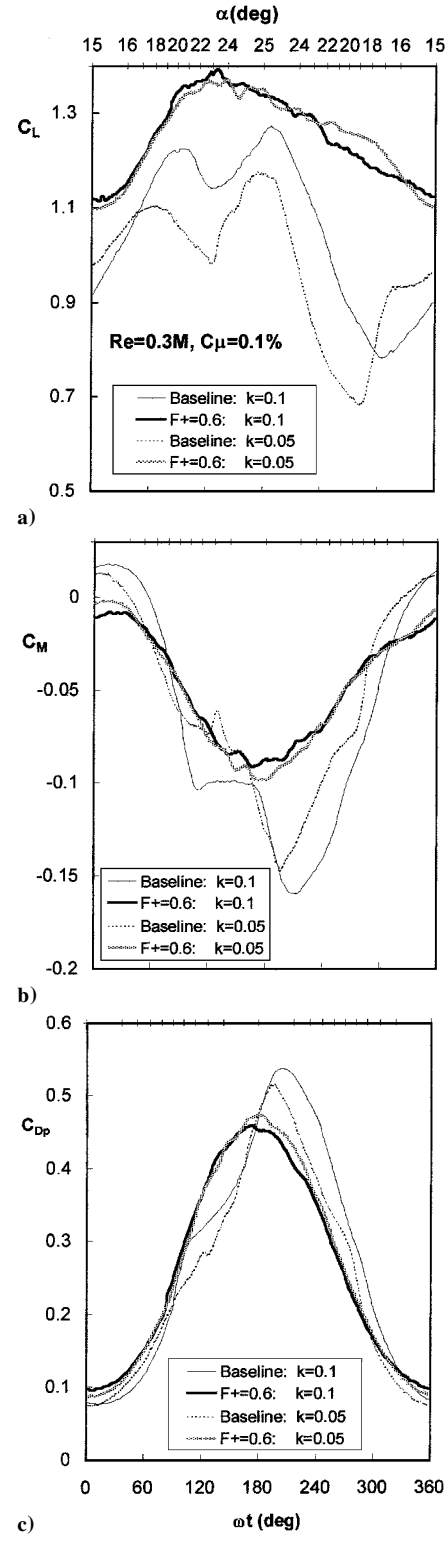

Fig. 13 Effect of airfoil oscillation rate on excitation effectiveness, $F^+ = 0.6$.

excursions in baseline instantaneous data are present. This is particularly evident from the lift data, which exhibit large excursions during the downstroke. Flow visualization data of Piziali[35] show that dynamic stall has a strong three-dimensional character, and this may explain the large excursions evident here. Excitation, on the other hand, significantly reduces the scatter associated with the downstroke data. Figures 14a–14c also indicate the rms associated with phase averaging the aerodynamic coefficients at $\alpha = 20$ deg on the downstroke. This emphasizes the disparity between baseline and excited cases and calls into question the validity of two-dimensional

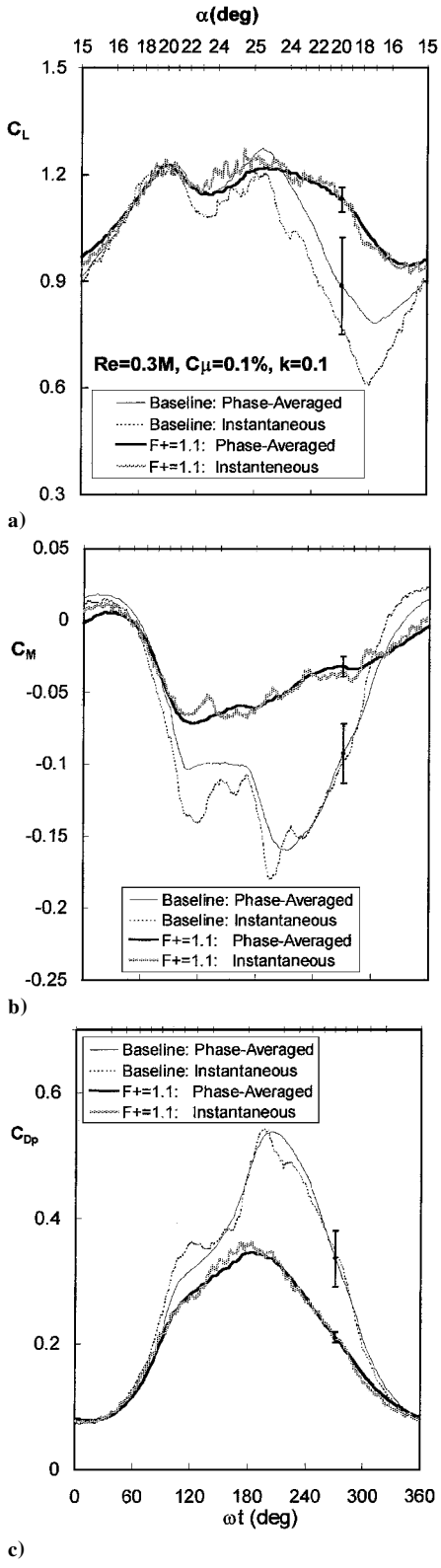

Fig. 14 Effect of excitation on instantaneous aerodynamic loads, F^+ = 1.1.

modeling of baseline dynamic stall.[21,22] On the other hand, two-dimensional slot excitation increases the spanwise coherence of the resulting LCSs, which significantly reduces cycle-to-cycle aberrations.

V. Conclusions

This paper outlined the parameters affecting separation control and demonstrated that they are similar under dynamic and static conditions. This characterization provided the key to understanding dynamic stall control by illustrating the large timescale (or frequency) disparity between the destructive DSV and the controlling LCSs.

A detailed study of the mechanisms of dynamic stall control on an airfoil revealed the following principal conclusions.

1) Excitation effectively removed the DSV and significantly attenuated trailing-edge separation.

2) Phase-averaged dynamic pressure distributions at maximum incidence were almost identical to static data under the same excitation conditions. The comparison improved further with increasing excitation frequency.

3) The generation and advection of LCSs over the airfoil surface at maximum incidence were similar, with differences in amplitude and phase velocity diminishing with increasing excitation frequency.

4) Excitation rendered the aerodynamic coefficients effectively independent of airfoil oscillation rate k.

5) Oscillations in aerodynamic coefficients induced by the excitation were insignificantly small when compared with phase-averaged quantities.

6) Excitation effectively eliminated the large instantaneous post-stall excursions, typical of the baseline aerodynamic coefficients, resulting in small differences between instantaneous and phase-averaged data.

Acknowledgments

This work was sponsored in part by a Grant from the Research and Development Office of the Israel Ministry of Defense, monitored by A. Kuritzki, and is an assigned task of the U.S./Israel MOA on rotorcraft aeromechanics. Assistance from the Tel Aviv University Aerolab staff and graduate students is gratefully acknowledged.

References

[1]Katz, Y., Nishri, B., and Wygnanski, I., "The Delay of Turbulent Boundary Layer Separation by Oscillatory Active Control," *Physics of Fluids 1*, 1989, pp. 179–181.

[2]Nishri, B., and Wygnanski, I., "Effects of Periodic Excitation on Turbulent Separation from a Flap," *AIAA Journal*, Vol. 36, No. 4, 1998, pp. 547–556.

[3]Seifert, A., Darabi, A., and Wygnanski, I., "Delay of Airfoil Stall by Periodic Excitation," *Journal of Aircraft*, Vol. 33, No. 4, 1996, pp. 691–698.

[4]Schubauer, G. B., and Skramstad, H. K., "Laminar Boundary Layer Oscillations and Transition on a Flat Plate," NACA Rept. 909, 1948.

[5]Collins, F. G., and Zelenevitz, J., "Influence of Sound upon Separated Flow over Wings," *AIAA Journal*, Vol. 13, No. 3, 1975, pp. 408–410.

[6]Brown, G. L., and Roshko, A., "On Density Effects and Large Structure in Turbulent Mixing Layers," *Journal of Fluid Mechanics*, Vol. 64, 1974, p. 775.

[7]Oster, D., Wygnanski, I., Dziomba, B., and Fiedler, H., "The Effect of Initial Conditions on the Two-Dimensional, Turbulent Mixing Layer," *Structure and Mechanics of Turbulence*, edited by H. Fiedler, Lecture Notes in Physics, Vol. 75, Springer-Verlag, Berlin, 1978, pp. 48–64.

[8]Seifert, A., Bachar, T., Koss, T., Shepshelovich, M., and Wygnanski, I., "Oscillatory Blowing, a Tool to Delay Boundary Layer Separation," *AIAA Journal*, Vol. 31, No. 11, 1993, pp. 2052–2060.

[9]Naveh, T., Seifert, A., Tumin, A., and Wygnanski, I., "Sweep Effect on Parameters Governing Control of Separation by Periodic Excitation," *AIAA Journal*, Vol. 35, No. 3, 1998, pp. 510–512.

[10]Seifert, A., and Pack, L. G., "Oscillatory Control of Separation at High Reynolds Numbers," AIAA Paper 98-0214, Jan. 1998.

[11]Hites, M., Nagib, H., Sytsma, B., Wygnanski, I., Seifert, A., and Bachar, T., "Lift Enhancement Using Pulsed Blowing at Compressible Flow Conditions," 50th Annual Meeting of the American Physical Society's Division of Fluid Dynamics, Nov. 1997.

[12]Seifert, A., Bachar, T., Wygnanski, I., Kariv, A., Cohen, H., and Yoeli, R., "Application of Active Separation Control to a Small Unmanned Air Vehicle," *Journal of Aircraft*, Vol. 36, No. 2, 1999, pp. 474–477.

[13]Carr, L. W., "Progress in the Analysis and Prediction of Dynamic Stall," *Journal of Aircraft*, Vol. 25, No. 1, 1988, pp. 6–17.

[14]Carr, L. W., and McAlister, K. W., "The Effect of a Leading-Edge Slat on the Dynamic Stall of an Oscillating Airfoil," AIAA Paper 83-2533, 1983.

[15]Yu, Y. H., Lee, S., McAlister, K. W., Tung, C., and Wang, C., "Dynamic Stall Control for Advanced Rotorcraft Application," *AIAA Journal*, Vol. 33, No. 2, 1995, pp. 289–295.

[16]Weaver, D., McAlister, K. W., and Tso, J., "Suppression of Dynamic Stall by Steady and Pulsed Upper-Surface Blowing," AIAA Paper 98-2413, June 1998.

[17]Addington, G. A., Schreck, S. J., and Luttges, M. W., "Static and Dynamic Flowfield Development About a Porous Suction Surface Wing," AIAA Paper 92-2628-CP, 1992.

[18]Shih, C., Lourenco, L., Van Dommelen, L., and Krothapalli, A., "Unsteady Flow Past an Airfoil Pitching at a Constant Rate," *AIAA Journal*, Vol. 30, No. 5, 1992, pp. 1153–1161.

[19]Carr, L. W., Chandrasekhara, N. J., and Brock, N. J., "Quantitative Study of Compressible Flow on an Oscillating Airfoil," *AIAA Journal*, Vol. 31, No. 4, 1994, pp. 892–898.

[20]Wilder, M. C., Chandrasekhara, M. S., and Carr, L. W., "Transition Effects on Compressible Dynamic Stall of Transiently Pitching Airfoils," AIAA Paper 93-2978, July 1993.

[21]Ekaterinaris, J. A., and Menter, F. R., "Computation of Oscillating Airfoil Flows with One- and Two-Equation Turbulence Models," *AIAA Journal*, Vol. 32, No. 12, 1994, pp. 2359–2365.

[22]Ko, S., and McCroskey, W. J., "Computations of Unsteady Separating Flows Over an Oscillating Airfoil," *AIAA Journal*, Vol. 35, No. 7, 1997, pp. 1235–1238.

[23]Hassan, A. A., "Numerical Simulations and Potential Applications of Zero-Mass Jets for Enhanced Rotorcraft Aerodynamic Performance," AIAA Paper 98-0211, Jan. 1998.

[24]Carr, L. W., Chandrasekhara, M. S., Wilder, M. C., and Noonan, K. W., "The Effect of Compressibility on Suppression of Dynamic Stalls Using a Slotted Airfoil," AIAA Paper 98-0332, Jan. 1998.

[25]Greenblatt, D., Seifert, A., and Wygnanski, I., "Dynamic Stall Management by Oscillatory Forcing," *Euromech Colloquium 361: Active Control of Turbulent Shear Flows*, Technische Universität, Berlin, 1997.

[26]Greenblatt, D., and Wygnanski, I., "Dynamic Stall Control by Oscillatory Forcing," AIAA Paper 98-0676, Jan. 1998.

[27]Greenblatt, D., Darabi, A., Nishri, B., and Wygnanski, I., "Separation Control by Periodic Addition of Momentum with Particular Emphasis on Dynamic Stall," American Helicopter Society, Paper T3-4, April 1998.

[28]Greenblatt, D., and Wygnanski, I., "Dynamic Stall Control by Periodic Excitation, Part 1: NACA 0015 Parametric Study," *Journal of Aircraft*, Vol. 38, No. 1, 2001, pp. 430–438.

[29]Van Dommelen, L., and Shen, S. F., "The Spontaneous Generation of the Singularity in a Separating Laminar Boundary Layer," *Journal of Computational Physics*, Vol. 38, 1980, pp. 125–140.

[30]Choudhuri, P. G., Knight, D. D., and Visbal, M. R., "Two-Dimensional Unsteady Leading-Edge Separation on a Pitching Airfoil," *AIAA Journal*, Vol. 32, No. 4, 1994, pp. 673–681.

[31]Shih, C., Lourenco, L. M., and Krothapalli, A., "Investigation of Flow at Leading and Trailing Edges of Pitching-Up Airfoil," *AIAA Journal*, Vol. 33, No. 8, 1995, pp. 1369–1376.

[32]Walker, J. D. A., "Unsteady Boundary Layer Separation in Two Dimensional Flows," *Workshop on Supermaneuverability: Physics of Separated Flows at High Angle of Attack*, Lehigh University, Bethlehem, PA, April 1992.

[33]Greenblatt, D., "Dynamic Stall Control by Oscillatory Excitation," Ph.D. Dissertation, Dept. of Fluid Mechanics and Heat Transfer, Faculty of Engineering, Tel Aviv Univ., Ramat Aviv, Israel, Nov. 1999.

[34]Darabi, A., "The Effect of Oscillatory Blowing on a Stalling Airfoil," M.Sc. Thesis, Dept. of Fluid Mechanics and Heat Transfer, Faculty of Engineering, Tel Aviv Univ., Ramat Aviv, Israel, Nov. 1995 (In Hebrew).

[35]Piziali, R. A., "2-D and 3-D Oscillating Wing Aerodynamics for a Range of Angles of Attack Including Stall," NASA TM 4632, 1994.